Characterization of the ECLIPS Space Environments Simulation Facility

Kieran Wilson*, Miles Bengtson†, Jordan Maxwell‡, Álvaro Romero-Calvo§ and Hanspeter Schaub¶
Ann and H.J. Smead Aerospace Engineering Department, University of Colorado, Boulder, Colorado, 80303

The Electrostatic Charging Laboratory for Interactions between Plasma and Spacecraft (ECLIPS) research vacuum chamber facility has recently been developed as part of the Autonomous Vehicle Systems Laboratory at the University of Colorado Boulder. This experimental spacecraft charging research facility provides capability to conduct experiments relevant to charged astrodynamics in a space-like environment. The paper discusses the development, characterization, and present capabilities of the vacuum chamber, which includes a range of sources to provide electron, ion, and photon fluxes, a 3-axis motion stage, magnetic field control, and a variety of sensors. This state-of-the art facility has been used to conduct experiments on touchlessly sensing spacecraft potentials, electrostatic actuation experiments, development of a new type of electron gun, and will continue to be a unique facility for studying spacecraft electrostatics in the future.

I. Introduction

The complexities of the space environment and enormous cost and difficulty involved in in-situ experimentation necessitates the development of terrestrial facilities to explore interactions of interest to spacecraft charging. To this end, the Autonomous Vehicle Systems (AVS) Laboratory at the University of Colorado Boulder has recently developed the Electrostatic Charging Laboratory for Interactions between Plasma and Spacecraft (ECLIPS), a vacuum chamber facility pictured in Fig. 1 which is designed for conducting spacecraft charging experiments. This paper describes the motivation design, development, characterization, and capability of the ECLIPS vacuum chamber.

While facilities designed to simulate thermal and vacuum (TVAC) environments in space have become commonplace as a pre-flight requirement for any spaceflight mission, experimental facilities intended to study spacecraft charging are fairly rare. A notable example is the JUMBO chamber at the Air Force Research Laboratory (AFRL) in Albuquerque, New Mexico. Chambers such as this one, and similar facilities at Aerospace Corporation, are primarily used to evaluate the impact of the space environment on materials, electronics and other components intended for orbital use [1]. The Sirene facility at ONERA in France likewise provides a sophisticated testbed for characterizing material properties under space environment exposure [2]. Another facility at Utah State University is also focused on spacecraft charging impacts, and uses a variety of photon, electron and ion sources to evaluate the electronic properties of materials [3].

Rather than focusing on fundamental material science or flight qualification questions as many of these other facilities, the ECLIPS chamber aims to focus on charged astrodynamics phenomena, such as remote sensing of electrostatic potential or plasma wake dynamics. Charged astrodynamics has been studied for over 20 years to explore how touchless actuation enables novel methods of close proximity control of space objects [4, 5]. The original concepts of charged astrodynamics ranged from creating charged virtual static structures [6–9], rendezvous and docking strategies [10–12], to controlling spinning sets of charged spacecraft [13–16]. More recent research explores the uses of electrostatic forces between a charged controlled spacecraft and a second space object which is charged remotely through the use of an electron beam from the servicer craft. The resulting force leads to the concept of the Electrostatic Tractor and the motivation for a geosynchronous large debris reorbiting concept [17–20]. Instead of creating a fixed electrostatic force between the spacecraft, References 21–24 explore the use of modulated electrostatic force fields to detumble a spinning space object. All this prior work was based on analytical and numerical analysis. Linear charged relative motion control was experimentally explored in the AVS Lab using an air-bearing hover track built out of non-conducting material [25–27]. To study the charged relative rotation a different test bed was developed in the AVS lab that used

*Graduate Researcher, Ann and H.J. Smead Aerospace Engineering Department
†Graduate Researcher, Ann and H.J. Smead Aerospace Engineering Department
‡Graduate Researcher, Ann and H.J. Smead Aerospace Engineering Department
§Graduate Researcher, Ann and H.J. Smead Aerospace Engineering Department
¶Professor, Glenn L. Murphy Endowed Chair, Ann and H.J. Smead Aerospace Engineering Department, AIAA and AAS Fellow

(a) Original chamber, as received from AFRL **(b) Current chamber configurations**

Fig. 1 The ECLIPS experimental test facility

a custom rotating bearing which could transfer a charge onto a spinning test object, also in atmospheric conditions [28, 29]. However, both of these charged relative motion dynamics facilities impart a potential onto the object using an electrostatic power supply and have to contend with the ionization of the local atmosphere. To explore touchless actuation in a vacuum or space like environment a new test facility was required. Further, as identified in Reference 30, knowledge of the nominal charging both of the servicer and the second space object is critical when performing charged relative position station keeping. If the charge uncertainty is too large, then the resulting closed loop motion undergoes a bifurcation in its behavior leading to a collision. This a motivation for seeking touchless methods to sense the charge of a neighboring space object, along with improving safety during rendezvous [31–34] This capability has many uses beyond charged astrodynamics such as rendezvous and docking, orbital serving and assembly, etc. However, no current vacuum chamber research facility specializes in the study of electrostatic actuation and touchless sensing of electrostatics in a space environment. Thus the idea of the ECLIPS chamber was formed to explore these exciting research directions with experimental support.

The paper is structured as follows: discussion of general facility including environmental control systems (pumps for the vacuum environment and quasi-Helmholtz coils for the magnetic environment) is presented in Sec. II; sources used in the chamber, including electron, ion and photon sources and high voltage power supplies are covered in Sec. III, while electron, x-ray and other probes are discussed in Sec. IV. Section VI describes associated support and control equipment. It is our goal that by presenting a detailed overview of this chamber other similar facilities can draw from the unique features of ECLIPS, helping to improve the overall experimental spacecraft-plasma community.

II. General facility overview

A bell-jar style vacuum chamber with 75 cm in diameter and 1 meter in height, illustrated in Figure 1a, was donated to the AVS Laboratory by the Air Force Research Lab in 2016. The chamber is made of stainless steel and has an o-ring interface between the bell and the base, which has a $^1/_4 - 20$ hole grid to allow mounting within the chamber. General vacuum chamber best practices are followed whenever possible, including ultrasonic cleaning of components in isopropyl alcohol prior to installation, minimization of any materials known to outgas contaminants such as many plastics, and use of vented screws in any blind holes to avoid virtual leaks.

The chamber includes a two-stage pumping system, with an Agilent IDP-15 scroll pump and an Agilent 1001 turbomolecular pump, capable of achieving pressures in the 10^{-7}-10^{-6} Torr range. This chamber has been significantly modified, with the addition of a range of KF and CF flanges of varying diameters, which are used to accommodate a range of viewports, sources, probes and feedthroughs. The viewports facilitate visual observations of electrostatic actuation and related processes, as used extensively in, for example, Reference 35. A current view of the ECLIPS chamber is shown in Figure 1b.

Sudden power failure could prove catastrophic for the turbomolecular pump, as well as electron and ion guns. To guard against this eventuality, the facility is connected to an Uninterruptible Power Supply (UPS), which provides up to 20 minutes of battery-based runtime in the event of a power failure. This is more than adequate to allow the building's backup power generators to come online and continue to provide support power to critical systems. All mechanical parts and electronic components are connected to a common ground and checked before the execution of a chamber experiment. The common ground is established by a copper grounding bar, which in turn is connected to the building ground.

The top of the bell jar is raised and lowered by two column lift mechanisms that provide access to the chamber. These units, the FLT-12 from Progressive Automations, can provide up to 30 cm of vertical actuation with 2600 lbf (11500 N) of lifting capacity, and are controlled via wired remote that can be programmed to specific heights. Slotted flanges welded to the exterior of the chamber enable interaction with the column lift, and also ensure that the full weight of the chamber lid rests on the o-ring interface with the base for optimal sealing. Additionally, the two lifts are electronically controlled to ensure that the chamber lid is always lifted level, and the fully-constrained nature of the system ensures that the chamber lid is repeatably positioned between runs.

III. Sources

A series of sources for magnetic fields, photons, electrons and ions have been integrated into the chamber, enabling various components of the space environment to be simulated. In general, the high energy photon source (vacuum ultraviolet lamp) is used to stimulate photoelectric emission for charging and potential sensing applications, while the electron beam is used to generate secondary electrons, study charged beam dynamics and generate x-rays for material characterization and potential sensing. The ion beam is intended primarily for spacecraft wake studies and cleaning material samples.

A. Magnetic environment control system

Numerous vacuum experiments benefit from the ability to control the magnetic environment. Potential applications include the cancellation of Earth's magnetic field, the imposition of a LEO/GEO-like configuration, or the study of specific plasma regimes. Equivalent facilities have been developed at larger scales worldwide, such as the IABG's Magnetic Field Simulation Facility in Germany [36] or the NASA's Spacecraft Magnetic Test Facility in Maryland [37].

The system has been designed to generate a uniform, 3-axis controllable magnetic field in a 10 cm cubic region inside the vacuum chamber. Three pairs of coils arranged in a quasi-Helmholtz configuration are considered, with the vertical ones being located inside the chamber and the horizontal ones in the outside. The specifications are given in Table 1, where R is the coil radius, L is the coils separation, $I_{\max}$ is the maximum allowed current intensity, $B_{\max}$ is the maximum magnetic flux density, N is the number of wire turns, B_{step} is the resolution achieved by the controller, R_{e^-} is the electron gyro-radius, and T_{eq} is the equilibrium temperature with maximum current intensity, computed with a lumped heat transfer model. A 5A constant current JUNTEK DPM-8605 power source has been assumed. The horizontal coils are designed to cancel the Earth's magnetic field ($\approx$20-65 μT), while the vertical coils produce a stronger magnetic environment. This choice is motivated by the highly demanding geometrical constraints of the chamber.

Besides the Earth's influence, the coils should also compensate the magnetic disturbances produced by the instruments and hardware of the facility. A 3D Finite-Elements Model (FEM) testbed has been built in Comsol Multiphysics to simulate the magnetic environment of specific experiments. Figure 2 shows the geometry and mesh of the model, where

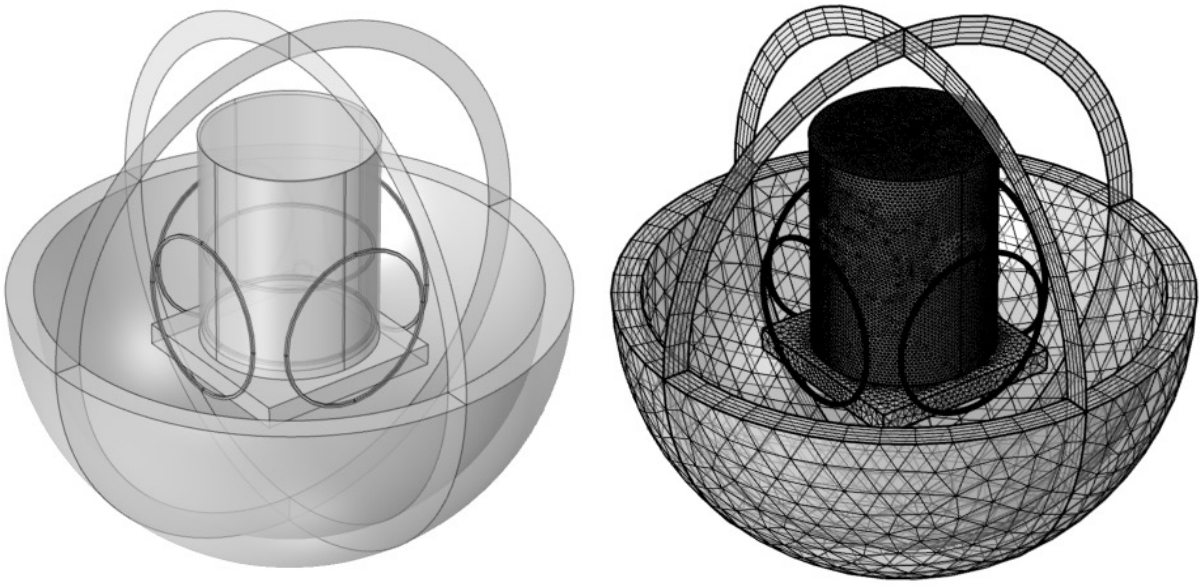

(a) Geometry **(b) Mesh**

Fig. 2 Magnetic FEM testbed

simplified shapes are employed to minimize the computational cost and an *infinite element domain* is implemented in the external contour. The chamber is made of stainless steel, and is assumed to have a relative permeability of 1.002.

A case of application of the magnetic testbed is shown in Fig. 3. The purpose of the simulation is to quantify the magnetic disturbance induced by the IMG-300 UHV Inverted Magnetron Gauge (IMG) * while the internal coils operate at 5 A. The figure shows the magnetic flux density and the vertical deviation angle α of the magnetic flux density vectors in a radial cross-section passing through the center of the IMG. The inhomogeneous field distribution reflects the strong influence of the IMG, that may disturb sensitive experiments.

B. Vacuum Ultraviolet Lamp

A Hamamatsu L10706 vacuum ultraviolet (VUV) light source, composed of a deuterium bulb with a MgF_2 window, is used to excite photoelectron emission from targets of interest. This source is flange mounted, and relies on an external air supply to provide cooling. The deuterium bulb and MgF_2 window result in a peak emission wavelength of 160 nm, with a total emission range of 115 to 400 nm. This device requires a constant supply of cooling air, provided by a building-wide compressed air supply.

C. Electron Gun

The primary electron gun for the facility is a Kimball Physics EMG-4212D, capable of accelerating electrons up to 30 keV. Figure 4 shows the electron gun mounted to the chamber. A phosphor screen (a Kimball Physics Rugged

*https://www.agilent.com/en/products/vacuum-technologies/vacuum-measurement/transducers/img-300-uhv-inverted-magnetron-gauge (Consulted on 06/26/2020)

Coils	R [mm]	L [mm]	I_{max} [A]	B_{max} [μT]	N[#]	B_{step} [nT]	R_{e^-} [cm]	T_{eq} [°C]
Internal	298	298	5	600	40	121	56	59
External	298	760	5	60	12	10	562	48

Table 1 Preliminary magnetic control system configuration

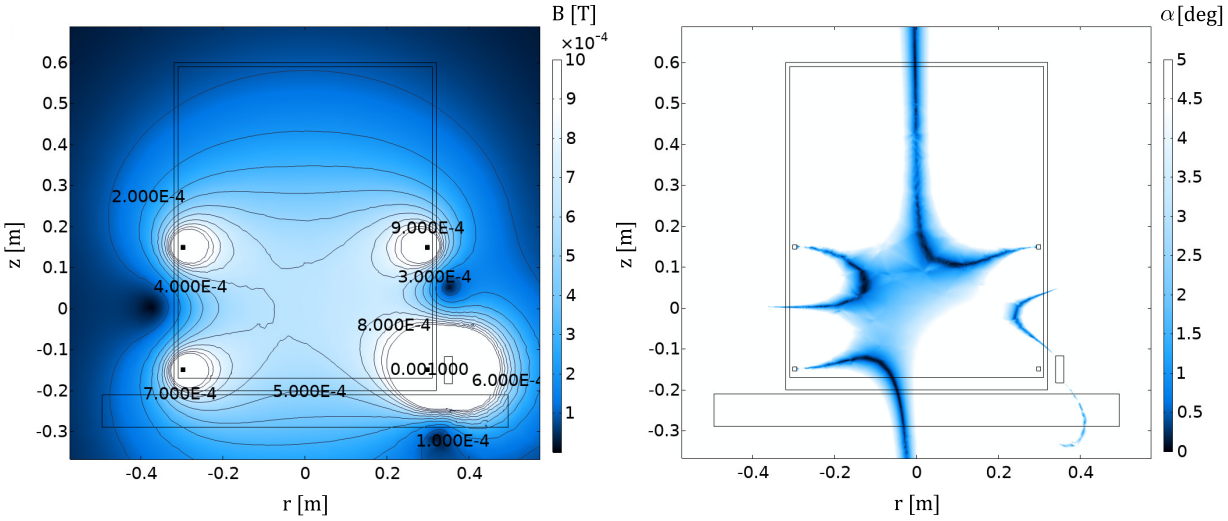

(a) Magnetic flux density **(b) Magnetic flux deviation from the vertical**

Fig. 3 Analysis of the magnetic disturbances induced by an IMG-300 UHV IMG in the radial cross-section passing through the center of the IMG.

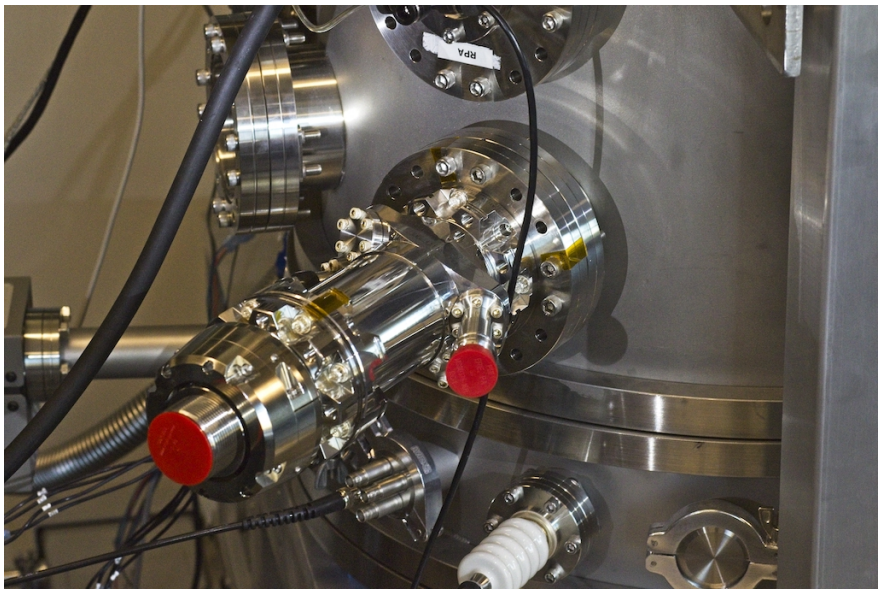

Fig. 4 Electron gun mounted onto the side of the ECIPS chamber

Phosphor Screen, diameter 3.8 cm) is used for visual identification of the beam position. The beam location and focus can be adjusted through optics integrated in the electron gun. Figure 5a illustrates the energy spectrum of the electron gun as observed by the RPA, for a nominal electron beam energy of 800V. The energy spreading visible in this plot is a result of both energy spreading within the electron gun, and also due to effects within the RPA. Reference [38] describes an analysis of in-detector energy spreading, and finds that $\approx$ 20V of spread can be expected at potentials of 1000V. The results shown in Fig. 5a are therefore consistent with a well-homogenized beam, with very little energy spreading not explained by the detector physics.

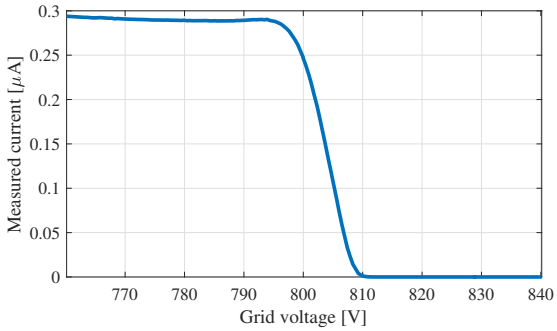

(a) RPA trace of electron beam set to a nominal 800V

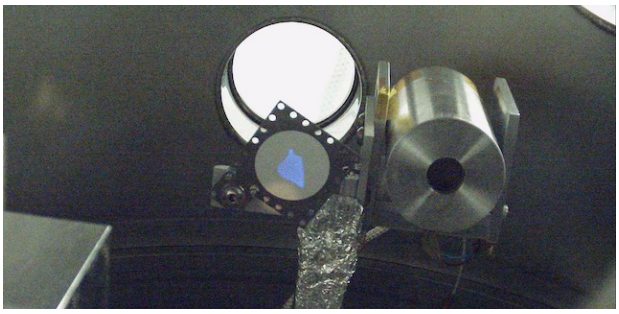

(b) Phosphor screen illustrating the size and shape of the electron beam (in blue). The RPA is mounted to the right of the screen [39].

Fig. 5 Electron beam characteristics

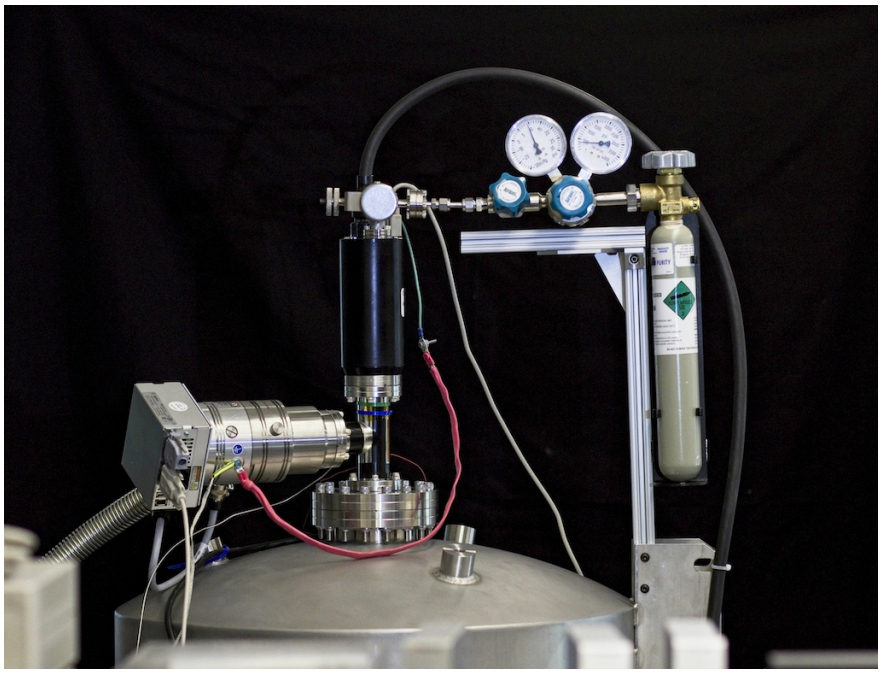

Fig. 6 Illustration of the ion gun setup on the top of the chamber.

D. Ion Gun

A 1402 Ion Gun from Non Sequitur Technologies provides the ability to clean samples while under vacuum, conduct charging experiments via positive charge irradiation, and simulate a Low Earth Orbit (LEO) like plasma flow. The ion gun is mounted vertically on top of the chamber, as shown in Figure 6. The source generates an ion beam continuously variable in energy from 5 eV to 3 keV with maximum beam current of 5 µA. A dedicated pumping system — consisting of a small turbomolecular pump backed by its own scroll pump — removes neutral elements not ionized in the gun to minimize charge exchange and similar interactions.

Figure 7 shows a beam map taken at 1 keV roughly 0.3 m below the ion gun barrel. Given these parameters, the beam diameter is roughly 1 cm, which is significantly larger than the aperture in the ion gun. The spreading of the beam farther away from the source is a result of spacecharge repulsion between ions in the beam. For operations such as sample cleaning this spreading effect may be desirable, but can be mitigated by neutralizing the beam with electron filaments for high-precision experiments. The offset between the coordinate-system origin and beam center seen in Fig. 7 is a result of misalignment between the ion optics in the gun and the motion stage. Both these components can be

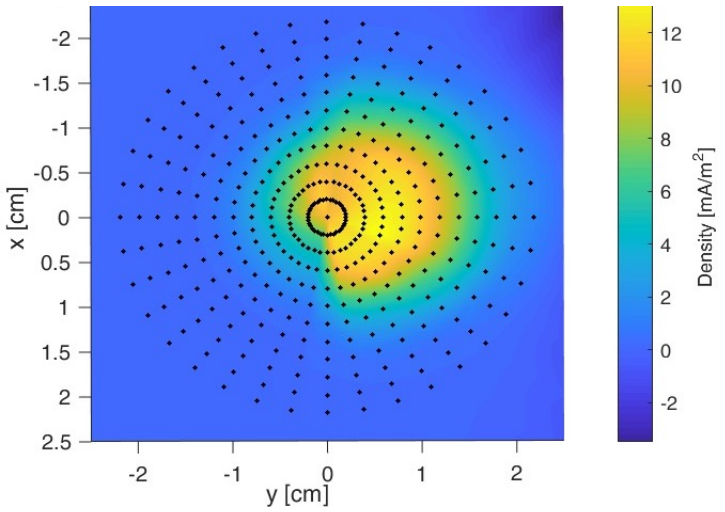

Fig. 7 Ion beam map at 1 keV

Table 2 Final ion beam expander design parameters

$\mathcal{E}_0$ **[eV]**	V_1 [V]	V_2 [V]	V_3 [V]	L_1 [Cm]	L_2 [Cm]	L_3 [Cm]	r_0 [Cm]	M
40	-210	39	40	14	5	14	0.1	35

tuned to achieve the desired alignment.

LEO simulation is achieved with the 1402 ion gun via introduction of ion optics. The notional system diagram is shown in Fig. 8. The ion beam enters the optics a short distance after exiting the source, is expanded by the electric fields within the optics, and then neutralized with electron filaments at the optics exit to mitigate further spacecharge spreading as the ion front flows past a given probe.

Given the extremely narrow beam diameter at the source ($\sim$ 1 mm), designing optics that produce a wide enough beam for experiments is challenging. Figure 9 shows a diagram of the optics. This "thick-lens" design is chosen over others because of its greater capacity to expand the beam. Nevertheless, the beam cannot practically be expanded more than about 10 times using the optics' electric fields, as excessive potentials are required. Instead, the spacecharge effect is leveraged to assist in the spreading of the beam.

Simulations run in SIMION — a ray-tracing program designed for design of plasma optics — provide an indication of the beam coherence after passing through optics. The lengths and potentials L_i and V_i are tuned such that an output beam is expanded to $\sim$3.5 cm. All simulation parameters are provided in Table 2. Note that this 35x expansion would not be feasible given only the optics. Figure 10 shows the collimation of the beam after expansion.

The SIMION simulation assumes a perfectly collimated, mono-energetic beam input to the optics. Theoretically, the properties shown in Fig. 2 should produce a highly collimated beam (i.e. particles should have no transverse velocity) but the spacecharge spreading effect discussed previously is complex and therefore cannot be easily accounted for. This is the reason for the $\sim$10% transverse velocity ratio near the beam edge. SIMION's spacecharge model is an approximation only, so optical properties of the beam expander will need to be iterated after construction and testing.

E. Broad spectrum electron gun

A unique capability of the system here is the presence of a broad spectrum electron gun, capable of mimicking the electron environment in a space plasma. Unlike traditional electron guns which generate monoenergetic beams, this device is designed to emit electrons at a range of energies simultaneously, currently at energies up to 9 keV. The physics, mode of operation and design of the system are described in detail in Reference [40]. This capability enables valuable investigations that cannot be adequately simulated through the use of monoenergetic electron beams, such as evaluating the emission of x-rays from a target due to the plasma environment, or investigating the charging behavior of a material under space-like electron environments.

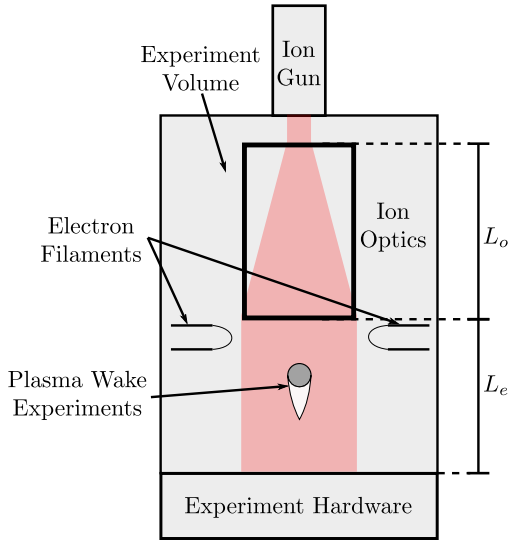

Fig. 8 Schematic diagram of LEO plasma simulation

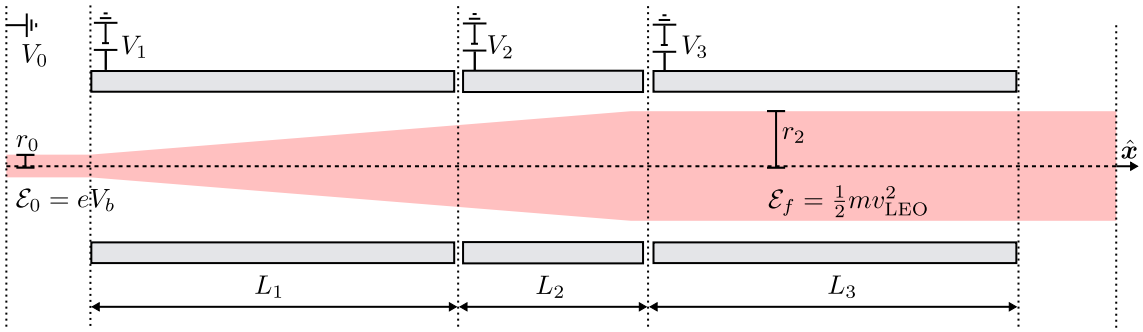

Fig. 9 Ion beam expander diagram

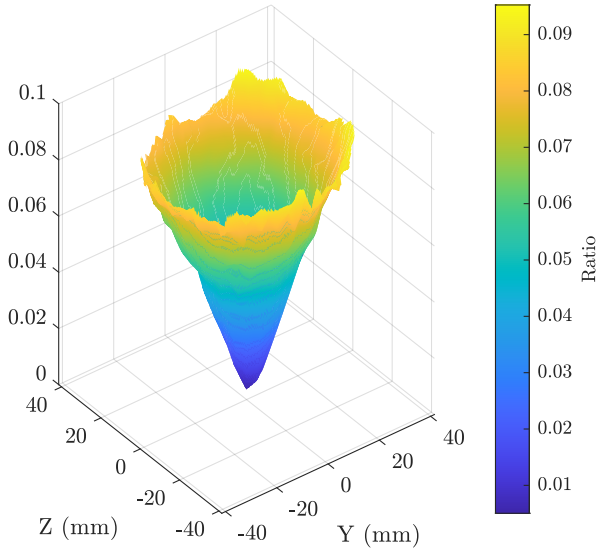

Fig. 10 Ratio of transverse to axial velocity for the ion gun.

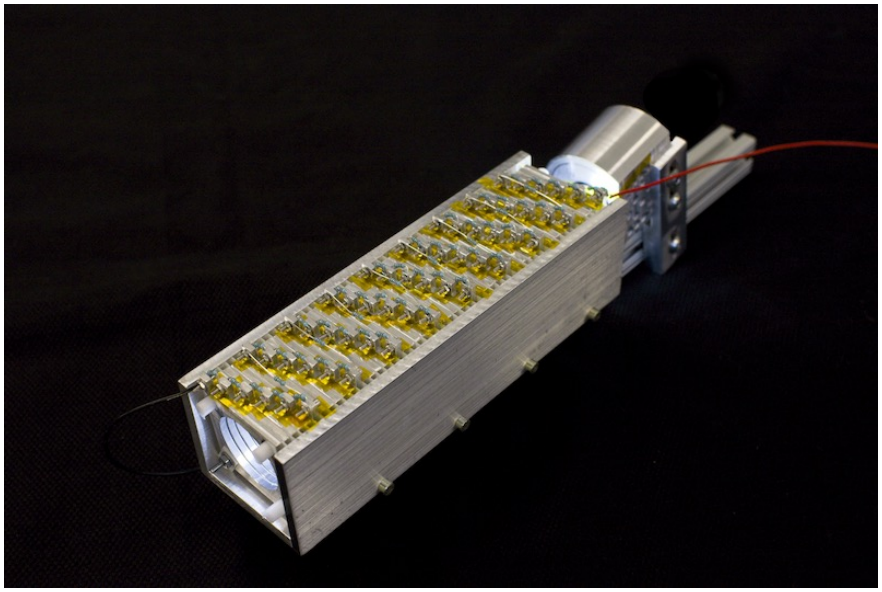

Fig. 11 Broad spectrum electron gun.

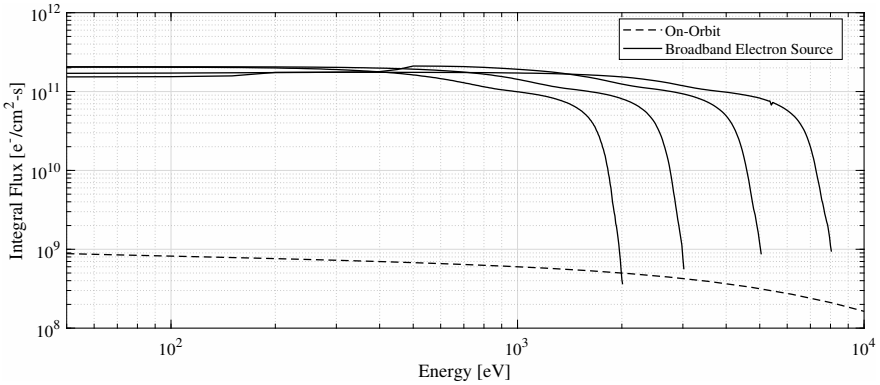

Fig. 12 Output spectra for broad-spectrum electron gun set to different energies.

Figure12 illustrates sample spectra that can be generated from this electron gun, distributing electrons in a wide range of energies compared with the rapid drop seen for the monoenergetic spectrum in Figure 5a. This generates an electron flux approximately two orders of magnitude greater than a comparable orbital environment, enabling material aging and exposure studies to be conducted in an accelerated manner. The spectra can be tuned to match a desired curve shape, and the maximum energy can likewise be adjusted. Work is underway to test the device at up to 30 keV emission energies, with plans for a maximum energy of 100 keV in future iterations.

IV. Probes

A series of sensors are used to ensure nominal operation of the chamber, and are not specific to any particular experimental configuration. These include an inverted magnetron gauge (Agilent IMG-100) for high vacuum pressure measurement (below 10^{-3} Torr), and an Agilent ConvecTorr gauge for high pressure measurement (from atmosphere to 10^{-4} Torr). Both gauges are controlled by dedicated cards in an Agilent XGS-600 gauge controller, and in tandem can provide accurate measurements of chamber pressure for the full range of obtainable pressures. Pressure gauges are complimented by a residual gas analyzer to monitor species in the chamber. Additionally, cameras are used to monitor and provide feedback on the position of in-chamber elements, while a phosphor screen is used for visual validation of electron beam alignment.

A Stefan-Mayer 3-axis FLC3-70 fluxgate magnetometer is used to measure magnetic fields in the range of $\pm 200\,\mu$T

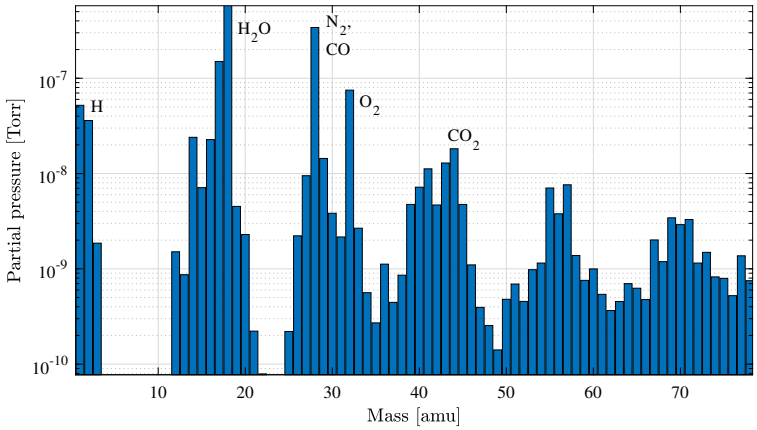

Fig. 13 RGA spectrum from 0-80 amu.

and DC to 1 kHz. This instrument is compact (a cylinder 3 cm in length and 1 cm in diameter) and vacuum rated, so it can be operated within the chamber and located at any point of interest. A full characterization of the magnetic field environment in the chamber is planned.

In addition to these system-level instruments, there are three probes which are used extensively in the course of conducting experiments in the chamber, and so are treated in more detail: a residual gas analyzer, an electron energy analyzer, and an x-ray spectrometer. The translation system used to position components in the chamber is also discussed here.

A. Residual Gas Analyzer

An Stanford Research Systems residual gas analyzer with a 200 amu range (SRS RGA-200) is used to monitor the molecular environment in the chamber during operations, and can provide useful diagnostic information in cases of high outgassing (as has been observed during extended stepper motor operation). Figure 13 illustrates a sample spectrum collected during nominal chamber operation after using the turbomolecular pump over night. Chamber base pressure at this time was 1.6×10^{-6} Torr; the lowest chamber base pressure observed has been $\sim 5 \times 10^{-7}$ Torr after an extensive remodel and cleaning process. Several significant contaminant species are labeled on the RGA spectrum, with air constituents ($N_2, O_2, CO_2/CO$) and water vapor (H and H_2O) being the most significant. These species account for over 70% of the residual partial pressure in the chamber at this time. Partial pressure contributions for species over 80 amu are typically on the order of 10^{-9} Torr, and have a relatively uniform pattern consistent with a "hydrocarbon forest" of high mass species. These are likely the result of residual oils from machining processes, as well as oils from pumps and off gassing plastics (although these are used only sparingly).

The residual carbon-bearing species have been observed resulting in brown discoloration on the phosphor screen, a result of Electron-Beam Induced Deposition (EBID) of those species onto the screen. This effect has also been observed after extended, low-energy use of the electron gun on aluminum target plates.

The pumps used for this system enable pumping down from atmosphere to $\sim 10^{-6}$ Torr in under 3 hours, enabling rapid advancement of experimental campaigns. While these pressures are acceptable for any equipment in the chamber, the occasional EBID of carbon-bearing species during electron beam use may lead to the addition of Getter plates in the future to reduce the partial pressure of high mass residual species.

B. Electron spectrum measurement

A custom electron energy analyzer has been built for the ECLIPS facility. The electron energy analyzer is a gridded Faraday cup design with a 1.2 cm diameter circular aperture. The device consists of a front grounded grid and a second discriminating grid to which high voltages can be applied. The discriminating grid creates an approximately equipotential plane and the front grid contains the electric fields inside the instrument. When no voltage is applied to the discriminating grid, an electron with any energy can pass through the instrument and into the detector. As a negative voltage, V, is applied, electrons with energies less than eV cannot overcome the potential barrier and thus are

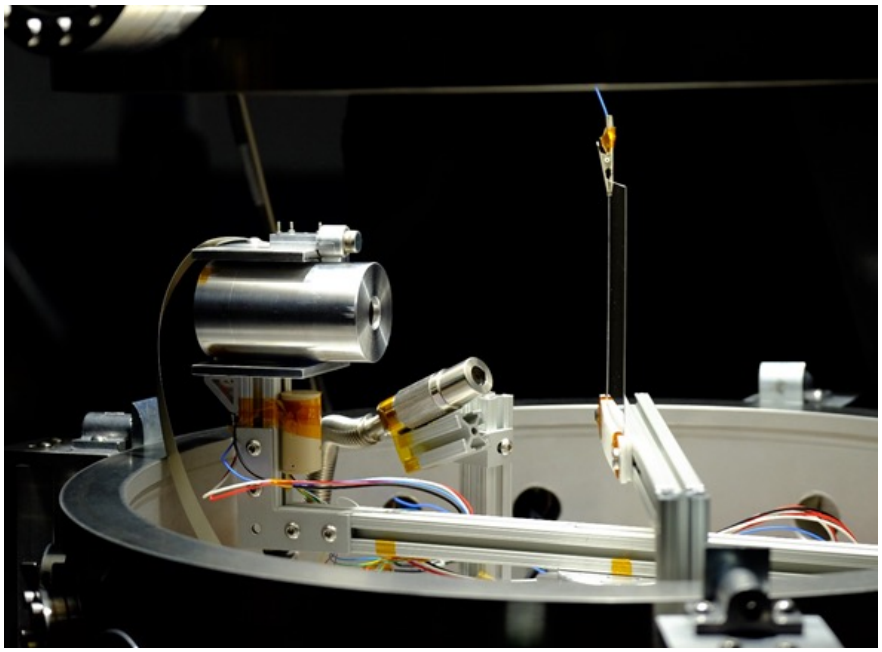

Fig. 14 Example experimental setup in chamber. RPA and x-ray detector seen on the left, VUV light in center, and target inconel plate connected to a HVPS on right.

repelled from the detector. Thus, by sweeping through voltages applied to the grid, the electron energy distribution is obtained. The collector itself is a hollow cylinder (closed at the back) which helps to prevent secondary or backscattered electrons generated on the collector from escaping back out the front of the instrument. The current is recorded using a Keithley 2401 SourceMeter picoammeter and one of the high-voltage power supplies is used to apply voltages to the discriminating grid. Several noise floor measurements have been taken in which the electron energy analyzer is installed in the chamber, but none of the sources are turned on, so there is no source of electrons. The measured noise current of the electron energy analyzer and picoammeter system has a mean of 0.0124 nA and a standard deviation of 0.0339 nA.

C. X-ray spectrometer

X-ray spectrum measurement is achieved through the use of an Amptek X123 X-ray spectrometer with a 6 mm^2 Si-PIN diode sensor. This unit is compact, lightweight and low-power, which reduces the amount of heat that must be removed from the system when operating in the vacuum chamber. In addition, this detector has spaceflight heritage as the primary instrument on the Mini-XSS solar observatory mission [41]. Detector calibration was accomplished in atmospheric conditions with an Fe-55 radioisotope source. This isotope emits X-rays at two energies, 5.89 and 6.49 keV, which are used to create a linear calibration for the detector under specific operating settings. The detector also has a 0.0254 mm thick beryllium frontal window. This beryllium window prevents stray photons from entering the detector, effectively attenuating any photons below 0.9 keV . In addition, the detector efficiency also decreases as the energy increases above 12 keV, due to photons passing through the active volume of the Si-PIN detector without depositing all of their energy [42].

The noise threshold of the detector increases with increasing temperature, so an integrated thermoelectric cooler is used to maintain acceptably low noise levels. For these experiments a temperature of 240K was maintained at the diode. While this represented somewhat higher noise and reduced resolution relative to the minimum achievable temperature of 217K, the temperature could be maintained for several hours at a time in the vacuum environment without running into thermal saturation of the heat sink. Therefore, long duration sweeps and experiments could be conducted without detector characteristics varying during testing.

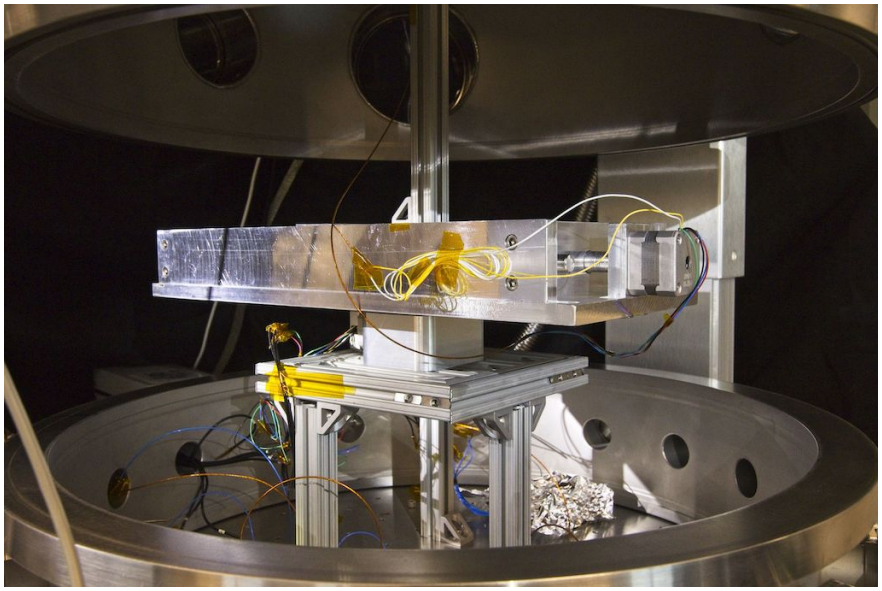

Fig. 15 Rotational stage (center) with translational stage mounted atop it.

D. Motion stages

Many experiments conducted in the ECLIPS facility have geometrical dependencies, whether a desire to sample electron populations at different points relative to a target, or examine the structure of a spacecraft wake under different charging conditions. This led to the development of a unique 3-axis translation system, with axes moving according to cylindrical coordinates, shown in Fig. 15. A rotational stage (Newmark Systems RM-3) is mounted on the base and then two custom-built linear stages (one horizontal and one vertical, using the same vac-safe stepper motors as the Newmark Systems RM-3 rotary stage) are mounted on the rotational stage, allowing for any arbitrary movement of be conducted in the chamber. The cylindrical design was chosen to maximize the use of space within the cylindrical chamber, allowing translations right up to the chamber walls in each direction. The position of each stage is measured by linear and rotary high-vacuum Renishaw Tonic encoders[†] with 5 μ m resolution. The encoders are connected to the LabView interface, and feed a closed-loop position control.

The steppers quickly warm up during operation in vacuum, outgassing primarily water with some contribution from carbon dioxide. For this reason, an Agilent XGS-600 vacuum gauge controller [‡] connected to the IMG pressure sensor keeps track of the pressure in the chamber and disconnects the steppers when a predetermined threshold is reached. This is important to ensure a safe operation of delicate components, such as electron or ion sources, rated for use only below 10^{-6} Torr.

V. Power systems

A major focus of chamber research is on spacecraft charging, and in particular the detection of charging remotely. This requires the ability to control the potential of a range of systems, from the RPA grids to a target plate, simultaneously. Therefore, a series of power supplies are integrated into the chamber facility, as seen in Figure 16. Two Matsusada AU-30R1 high voltage power supplies (HVPS) provide high quality potentials up to 30 kV. These units are controlled via fiber optic connections to the primary computer, reducing the potential for interference. In addition to the Matsusada power supplies, several other HVPS units are available for experiments, including two Spellman CZE2000 units (maximum voltage of 30 kV), and two SL300 high current power supplies with a maximum voltage of 3 kV at up to 300 Watts.

Monitoring of potentials is achieved through a Kiethly DMM6500 (for potentials up to 1000V), while a Keithley 2401 SourceMeter picoammeter is used to monitor current. Both are computer controlled, enabling rapid measurements

[†] `https://www.renishaw.com/en/tonic-encoder-series--37824` (Consulted on 11/23/2020)

[‡] `https://www.agilent.com/en/product/vacuum-technologies/vacuum-measurement/gauge-controllers/xgs-600-vacuuim-gauge-controller` (Consulted on 11/23/2020)

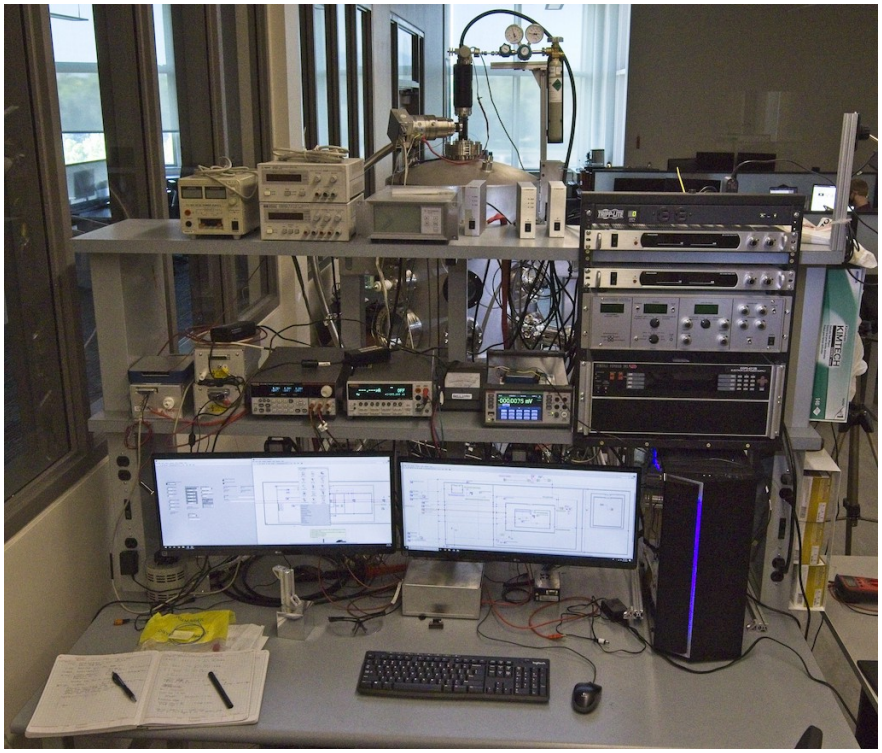

Fig. 16 Power supplies and control infrastructure for the chamber. The server rack at top right contains HVPS, and controllers for the electron and ion guns.

and development of control VIs that can feedback on detected currents or potentials (for instance, an experiment may aim to establish a fixed potential on a free-floating ungrounded plate through the use of the electron beam). Additionally, a low-voltage power supply, Keysight E3631A, is used to provide power for stepper motors.

VI. Control

All chamber systems are controlled via a central workstation computer and a series of LabView Virtual Instruments (VIs). A central program keeps track of the pressure level and issues an alert when it exceeds the safe operation environment. This may happen due to outgassing of high-temperature elements, such as stepper motors or coils, and can potentially degrade delicate hardware components. In addition, the central program assists the user in the pumping down and venting procedures, automating the operation of the IMG and making sure that all instruments have an appropriate configuration during these critical transitions.

The central program provides shortcuts to a set of standard sub-VIs. At the time of writing, those include a stepper control program employed to manually position the experiment, a software controller for the RGA, and a full interface for the electron gun. The user develops its own automation routine for a specific experiment, which runs separately from the chamber control system. However, an extensive library of sub-VIs is available to configure and use all the instruments in the chamber.

VII. Future Work

While enormous strides have been achieved over the past 4 years of facility development, a range of future improvements are planned. Notably, development of the magnetic actuators remains to be completed and integrated, with coils for the vertical axis currently under fabrication and installation anticipated in Q1 of 2021. Additionally, the translation stages will be upgraded with the new encoders, allowing tighter integration with the computer-based control systems and better estimation of probe positioning within the chamber. Ambient electron sources consisting of low-potential electrons emitted from filaments may be incorporated as part of future wake studies. Additionally,

the incorporation of getter plates are under consideration to minimize EBID carbon deposition that has been observed during extended low-energy electron beam use.

VIII. Conclusions

As with any large experimental facility, the development of the ECLIPS facility has involved the efforts of a large team over several years. These efforts have succeeded in developing a unique space environments simulation facility, with the ability to conduct a range of experiments in all areas of charged astrodyanmics research. Experimental campaigns using this facility have explored the electrostatic actuation of flexible structures [35], the impact of charged spacecraft structures on electron beam targeting and focusing [39], as well as the use of electron [33, 34] and x-ray [32, 43] methods for determining the electrostatic potential of an object remotely. Future work will expand on these investigations, with new capabilities added regularly.

Acknowledgements

The authors would like to thank Ryan Block and Charlie Lipscomb for their support in developing the magnetic coils and Dalton Turpen for his assistance with designing and fabricating numerous components. The valuable contributions of Dr. Joe Hughes in the early days of facility development are gratefully acknowledged. The AVS Laboratory is deeply grateful to AFRL for donating the original vacuum chamber and pumps, and feedback on operations and design decisions. This work was supported through Air Force Office of Scientific Research grant #FA9550-20-1-0025.

References

[1] "Jumbo Space Environment Simulation and Spacecraft Charging Chamber Characterization," Technical report, Air Force Research Laboratory, Space Vehicles Directorate, Albuquerque, New Mexico, 4 2015. URL `https://apps.dtic.mil/sti/pdfs/AD1000521.pdf`.

[2] Paulmier, T., Dirassen, B., Belhaj, M., Inguimbert, V., Duzellier, S., Pons, C., Rémaury, S., and Payan, D., "Experimental Test Facilities for Representative Characterization of Space Used Materials," *14th Spacecraft Charging Techology Conference*, Noordwijk, Netherlands, 2016.

[3] Dennison, J., Thomson, C., Kite, J., Zavyalov, V., and Corbridge, J., "Materials Characterization at Utah State University: Facilities and Knowledgebase of Electronic Properties of Materials Applicable to Spacecraft Charging," *8th Spacecraft Charging Technology Conference*, Huntsville, Alabama, 2003.

[4] Cover, J. H., Knauer, W., and Maurer, H. A., "Lightweight Reflecting Structures Utilizing Electrostatic Inflation," US Patent 3,546,706, October 1966.

[5] King, L. B., Parker, G. G., Deshmukh, S., and Chong, J.-H., "Study of Interspacecraft Coulomb Forces and Implications for Formation Flying," *AIAA Journal of Propulsion and Power*, Vol. 19, No. 3, 2003, pp. 497–505.

[6] Berryman, J., and Schaub, H., "Static Equilibrium Configurations in GEO Coulomb Spacecraft Formations," *Advances in Astronautical Sciences*, Vol. 120, American Astronautical Society, 2005, pp. 51–68. Paper No. AAS 05–104.

[7] Schaub, H., Hall, C., and Berryman, J., "Necessary Conditions for Circularly-Restricted Static Coulomb Formations," *Journal of the Astronautical Sciences*, Vol. 54, No. 3–4, 2006, pp. 525–541.

[8] Berryman, J., and Schaub, H., "Analytical Charge Analysis for 2- and 3-Craft Coulomb Formations," *AIAA Journal of Guidance, Control, and Dynamics*, Vol. 30, No. 6, 2007, pp. 1701–1710.

[9] Vasavada, H., and Schaub, H., "Analytic Solutions for Equal Mass Four-Craft Static Coulomb Formation," *Journal of the Astronautical Sciences*, Vol. 56, No. 1, 2008, pp. 17–40.

[10] Natarajan, A., Schaub, H., and Parker, G. G., "Reconfiguration of a Nadir-Pointing 2-Craft Coulomb Tether," *Journal of British Interplanetary Society*, Vol. 60, No. 6, 2007, pp. 209–218.

[11] Natarajan, A., and Schaub, H., "Orbit-Nadir Aligned Coulomb Tether Reconfiguration Analysis," *Journal of the Astronautical Sciences*, Vol. 56, No. 4, 2008, pp. 573–592.

[12] Natarajan, A., and Schaub, H., "Hybrid Control of Orbit Normal and Along-Track Two-Craft Coulomb Tethers," *Aerospace Science and Technology*, Vol. 13, No. 4–5, 2009, pp. 183–191. doi:10.1016/j.ast.2008.10.002, URL `http://dx.doi.org/doi:10.1016/j.ast.2008.10.002`.

[13] Wang, S., and Schaub, H., "Nonlinear Feedback Control of a Spinning Two-Spacecraft Coulomb Virtual Structure," *IEEE Transactions on Aerospace and Electronic Systems*, Vol. 47, No. 3, 2011, pp. 2055–2067. doi:10.1109/TAES.2011.5937282.

[14] Wang, S., and Schaub, H., "Nonlinear Charge Control for a Collinear Fixed Shape Three-Craft Equilibrium," *AIAA Journal of Guidance, Control, and Dynamics*, Vol. 34, No. 2, 2011, pp. 359–366. doi:10.2514/1.52117.

[15] Hogan, E., and Schaub, H., "Linear Stability and Shape Analysis of Spinning Three-Craft Coulomb Formations," *Celestial Mechanics and Dynamical Astronomy*, Vol. 112, No. 2, 2012, pp. 131–148. doi:10.1007/s10569-011-9387-6.

[16] Hogan, E., and Schaub, H., "Collinear Invariant Shapes for Three-Craft Coulomb Formations," *Acta Astronautica*, Vol. 12, 2012, pp. 78–89. doi:10.1016/j.actaastro.2011.10.020.

[17] Schaub, H., and Moorer, D. F., "Geosynchronous Large Debris Reorbiter: Challenges and Prospects," *The Journal of the Astronautical Sciences*, Vol. 59, No. 1–2, 2014, pp. 161–176.

[18] Hogan, E., and Schaub, H., "Space Weather Influence on Relative Motion Control using the Touchless Electrostatic Tractor," *Journal of Astronautical Sciences*, Vol. 63, No. 3, 2016, pp. 237–262.

[19] Hogan, E. A., "Impacts of Tug and Debris Sizes on Electrostatic Tractor Charging Performance," *Advances in Space Research*, Vol. 55, No. 2, 2014, pp. 630–638.

[20] Hogan, E. A., and Schaub, H., "Impacts of Hot Space Plasma and Ion Beam Emission on Electrostatic Tractor Performance," *IEEE Transactions on Plasma Science*, Vol. 43, No. 9, 2014, pp. 3115–3129.

[21] Schaub, H., and Stevenson, D., "Prospects Of Relative Attitude Control Using Coulomb Actuation," *Journal of the Astronautical Sciences*, Vol. 60, 2013.

[22] Bennett, T., Stevenson, D., Hogan, E., McManus, L., and Schaub, H., "Prospects and Challenges of Touchless Debris Despinning Using Electrostatics," *Advances in Space Research*, Vol. 56, No. 3, 2015, pp. 557–568.

[23] Bennett, T., and Schaub, H., "Touchless Electrostatic Three-Dimensional Detumbling of Large Axi-Symmetric Debris," *Journal of Astronautical Sciences*, Vol. 62, No. 3, 2015, pp. 233–253.

[24] Bennett, T., and Schaub, H., "Capitalizing On Relative Motion In Electrostatic Detumbling Of Axi-Symmetric Geo Objects," *6th International Conference on Astrodynamics Tools and Techniques (ICATT)*, Darmstadt, Germany, 2016.

[25] Seubert, C. R., and Schaub, H., "One-Dimensional Testbed for Coulomb Controlled Spacecraft Studies," *AAS/AIAA Spaceflight Mechanics Meeting*, Savannah, Georgia, 2009. Paper AAS 09–115.

[26] Seubert, C. R., and Schaub, H., "Electrostatic Force Model for Terrestrial Experiments on the Coulomb Testbed," *61st International Astronautical Congress*, International Astronautical Federation, Prague, CZ, 2010. Paper IAC-10.C1.1.9.

[27] Seubert, C. R., and Schaub, H., "Closed-Loop One-Dimensional Charged Relative Motion Experiments Simululating Constrained Orbital Motion," *AIAA Journal of Guidance, Control, and Dynamics*, Vol. 33, No. 6, 2009, pp. 1856–1865. doi:10.2514/1.48274.

[28] Stevenson, D., and Schaub, H., "Terrestrial Testbed for Remote Coulomb Spacecraft Rotation Control," *International Journal of Space Science and Engineering*, Vol. 2, No. 1, 2013, pp. 96 – 112.

[29] Stevenson, D., and Schaub, H., "Rotational Testbed for Coulomb Induced Spacecraft Attitude Control," *5th International Conference on Spacecraft Formation Flying Missions and Technologies*, Münich, Germany, 2013.

[30] Hogan, E., and Schaub, H., "Relative Motion Control for Two-Spacecraft Electrostatic Orbit Corrections," *AIAA Journal of Guidance, Control, and Dynamics*, Vol. 36, No. 1, 2013, pp. 240–249.

[31] Wilson, K., and Schaub, H., "X-Ray Spectroscopy for Electrostatic Potential and Material Determination of Space Objects," *IEEE Transactions on Plasma Science*, 2019.

[32] Wilson, K., Bengtson, M., and Schaub, H., "X-ray Spectroscopic Determination of Electrostatic Potential and Material Composition for Spacecraft: Experimental Results," *Space Weather*, Vol. 18, No. 4, 2020, pp. 1–10. doi:10.1029/2019SW002342.

[33] Bengtson, M., Hughes, J., and Schaub, H., "Prospects and Challenges for Touchless Sensing of Spacecraft Electrostatic Potential Using Electrons," *IEEE Transactions on Plasma Science*, 2019.

[34] Bengtson, M. T., and Schaub, H., "Remote Sensing of Spacecraft Potential at Geosynchronous Orbit using Secondary and Photo Electrons," *AIAA Scitech 2019 Forum*, 2019, p. 0311.

[35] Maxwell, J., Wilson, K., Hughes, J., and Schaub, H., "Multisphere Method for Flexible Conducting Space Objects: Modeling and Experiments," *AIAA Journal of Spacecraft and Rockets*, Vol. 57, No. 2, 2020, pp. 225–234. doi:10.2514/1.A34560.

[36] Kuegler, H., "Peformance improvement of the magnetic field simulation facility MFSA," *Proceedings of the 5th International Symposium on Environmental Testing for Space Programmes, Noordwijk (ESA SP-558, June 2004)*, 2004, pp. 407–414.

[37] Vernier, R., Bonalosky, T., and Slavin, J., "Goddard Space Flight Center Spacecraft Magnetic Test Facility Restoration Project," *23rd Space Simulation Conference Proceedings*, 2004. NASA/CP-2005-212775.

[38] Bengtson, M., "Electron Method for Touchless Electrostatic Potential Sensing of Neighboring Spacecraft," Ph.D. thesis, University of Colorado Boulder, 2015.

[39] Romero-Calvo, A., Cano-Gómez, G., and Schaub, H., "Electron beam expansion and deflection uncertainty for active spacecraft charging applications," *Proceedings of the 2021 AIAA SciTech Forum and Exposition*, 2021.

[40] Bengtson, M., Wilson, K., and Schaub, H., "Broad-Spectrum Electron Gun for Laboratory Simulation of Orbital Environments," *Proceedings of the 2021 AIAA SciTech Forum and Exposition*, 2021.

[41] Moore, C. S., Caspi, A., Woods, T. N., Chamberlin, P. C., Dennis, B. R., Jones, A. R., Mason, J. P., Schwartz, R. A., and Tolbert, A. K., "The Instruments and Capabilities of the Miniature X-Ray Solar Spectrometer (MinXSS) CubeSats," *Solar Physics*, Vol. 293, No. 2, 2018. doi:10.1007/s11207-018-1243-3.

[42] "XR-100CR Si-PIN x-ray detector," Tech. rep., Amptek, Inc., 2018.

[43] Wilson, K. T. H., Bengtson, M., and Schaub, H., "Hybrid Method of Remote Sensing of Electrostatic Potential for Proximity Operations," *IEEE Aerospace Engineering Conference*, Big Sky, MO, 2020.